Revision 1

Hydrous Species in Feldspars: a Reassessment Based on FTIR and SIMS

JED L. MOSENFELDER[1,2*], GEORGE R. ROSSMAN[1], AND ELIZABETH A. JOHNSON[3]

[1]Division of Geological and Planetary Sciences, California Institute of Technology, M/C 170-25, Pasadena, California 91125-2500, U.S.A.

[2]Department of Geology and Geophysics, University of Minnesota, 310 Pillsbury Drive SE, Minneapolis, Minnesota, 55455, U.S.A.

[3]Department of Geology and Environmental Science, James Madison University, 395 S. High St., MSC 6903, Harrisonburg, Virginia, 22807, U.S.A.

[*]E-mail: jmosenfe@umn.edu

ABSTRACT

Recent interest in hydrogen incorporation in feldspars has been driven by the potential of this common mineral species to record magmatic water contents. Accurate measurement of H concentrations in feldspars by Fourier transform infrared (FTIR) spectroscopy is hampered by the need to collect polarized spectra in at least three mutually perpendicular directions, which can be impractical for crystals characterized by small dimensions, polysynthetic twinning, and/or chemical zoning. SIMS is an attractive alternative to FTIR, offering high spatial resolution, high precision, and the feasibility of attaining low detection limits. In this study we compare FTIR and SIMS data for 19 feldspars, including plagioclase, anorthoclase, sanidine, microcline, and orthoclase. We present adjustments to previously published FTIR data on some of these samples. Our new SIMS and FTIR data are well correlated and we demonstrate the feasibility of quantitatively measuring H concentrations as low as 1-2 ppmw H_2O using SIMS. Combination of the new data together with re-evaluation of the NMR calibration of Johnson and Rossman (2003) indicates that the IR absorption coefficients for hydrous species in feldspar increase with decreasing frequency of their O-H absorptions, in accord with theory. We derive new molar integral IR absorption coefficients (I) for feldspars with the following hydrous species as defined by Johnson and Rossman (2003):

Type I and II H_2O (microcline and orthoclase): $I = 120,470 \pm 11,360\ L \cdot mol^{-1}{}_{H2O} \cdot cm^{-2}$

Type IIb OH (sanidine): $I = 150,000 \pm 15,000\ L \cdot mol^{-1}{}_{H2O} \cdot cm^{-2}$

Type IIa OH (plagioclase and anorthoclase): $I = 202,600 \pm 20,260\ L \cdot mol^{-1}{}_{H2O} \cdot cm^{-2}$

These absorption coefficients depend on critical assumptions with regards to SIMS matrix effects. If accurate, one important implication is that the H concentrations of plagioclase crystals

This is a preprint, the final version is subject to change, of the American Mineralogist (MSA)
Cite as Authors (Year) Title. American Mineralogist, in press.
(DOI will not work until issue is live.) DOI: http://dx.doi.org/10.2138/am-2015-5034

estimated in the literature are too high by up to a factor of two, requiring revision of previously estimated plagioclase-melt H partitioning coefficients.

INTRODUCTION

Feldspars are the most abundant minerals in the Earth's crust and have long been known to contain hydrous components within their structures, in the form of OH, H_2O, and/or NH_4^+ molecules (Wilkins and Sabine 1973; Solomon and Rossman 1979; 1988; Hofmeister and Rossman 1985a,b; 1986; Beran 1986, 1987; Müller, 1988; Behrens and Müller, 1995; Kronenberg et al. 1996; Xia et al. 2000; Johnson and Rossman 2003, 2004). Reported concentrations of structurally bound OH, H_2O, and NH_4^+ in this nominally anhydrous mineral (NAM) group range up to 915, 1350, and 1500 ppmw H_2O, respectively (Johnson 2006). Recent studies have shown the potential for using H concentrations in igneous plagioclase and anorthoclase to constrain the water contents of their host magmas, both in terrestrial volcanic rocks (Johnson 2005; Seaman et al. 2006; Hamada et al. 2011, 2013) and in lunar anorthosites (Hui et al. 2013). Although there are still some uncertainties in feldspar-melt H partition coefficients (Hamada et al. 2013), this technique holds great promise for complementing more traditional approaches to determining magmatic volatile contents, such as measuring the compositions of melt inclusions in phenocrysts (e.g., Blundy et al. 2006). However, one of the barriers to practical application of this method lies in accurately quantifying feldspar H concentrations, which are most typically measured using Fourier transform infrared (FTIR) spectroscopy. Because of the high degree of anisotropy of O-H bonding in feldspars, accurate FTIR is limited by the need to collect polarized spectra from three mutually perpendicular directions (Johnson and Rossman 2003). In practice, preparation of the appropriate sections for such measurements can be difficult when crystals are small and/or twinned or compositionally zoned, as commonly observed for phenocrysts or feldspars extracted from high-pressure experiments.

For the above reason, analysis by secondary ion mass spectrometry (SIMS) is an attractive proposition. Advantages of SIMS include high spatial resolution, apparent insensitivity to crystal orientation (Koga et al. 2003), high precision (e.g., Mosenfelder and Rossman 2013a,b) and the feasibility of attaining detection limits of 5 ppmw H_2O or even less (e.g., Hauri et al. 2002; Koga et al. 2003; Aubaud et al. 2007; Mosenfelder et al. 2011). In this study we conducted a cross comparison of FTIR and SIMS data for 19 feldspars of variable composition and structural state, including plagioclase, anorthoclase, sanidine, microcline, and orthoclase. Seven of our samples were previously investigated by Johnson and Rossman (2003), using both FTIR and nuclear magnetic resonance (NMR) spectroscopy. An additional 11 of the samples were previously measured using FTIR by Johnson and Rossman (2004), as part of a broad survey of hydrous species in igneous feldspars. In the present work we deliberately excluded feldspars containing obvious evidence for hydrous alteration products or fluid inclusions caused by subsolidus hydrothermal exchange, which are likely irrelevant to the study of volcanic phenocrysts. Moreover, as we have shown for olivine and pyroxene (Mosenfelder et al. 2011; Mosenfelder and Rossman 2013a), hydrous inclusions – even when not optically detectable – can lead to a high degree of scatter in SIMS measurements, complicating interpretation.

Due to limited data, Johnson and Rossman used their NMR and FTIR data to derive a universally applicable, integral IR absorption coefficient for absorption bands representing structurally bound H – both in the form of OH (in plagioclase/anorthoclase and sanidine, with mean wavenumbers of either ~3200 or ~3300 cm^{-1}, respectively) and H_2O (in microcline/orthoclase, with a mean wavenumber of ~3475 cm^{-1}). However, theoretical and experimental work (e.g., Paterson 1982; Libowitzky and Rossman 1997; Balan et al. 2008; Koch-Müller and Rhede 2010) suggests that there should be a difference in absorption coefficients for bands at these different wavenumbers. Johnson and Rossman's universally applicable value is supported by the excellent agreement between their NMR data and previous manometry (Hofmeister and Rossman 1985a,b) and NMR (Yesinowski et al. 1988) results. However, there were moderate uncertainties associated with H background subtraction of the NMR spectra, particularly for the samples with low H content (four plagioclases and one sanidine). Our cross calibration of FTIR and SIMS data allows us to place new constraints on the accuracy of the IR calibration and the wavenumber dependence of the absorption coefficient, while demonstrating the feasibility of performing highly precise SIMS measurements with a low detection limit (as low as 1-2 ppmw H_2O). We also detail some discrepancies between our new FTIR measurements and previous work and evaluate attendant implications for the IR calibration.

ANALYTICAL METHODS

Sample preparation and FTIR

Table 1 shows localities, general compositions (Ab-An-Or content), and FTIR data for the H-bearing feldspars and dehydrated feldspars (see SIMS section below) that we studied. More information about geologic settings and original references for the samples can be found in Johnson and Rossman (2003, 2004), and in Rossman (2011). We cut and polished new sections for SIMS, in some cases from the same crystals used previously and in other cases from different crystals from the same locality. FTIR spectra were re-measured in order to verify consistency with previous work and homogeneity in H contents. For GRR2651 we prepared a section from a different gem-quality crystal than the one used by Rossman (2011) for ^{40}Ar-^{39}Ar release experiments.

Crystals were oriented by morphology and cleavage where convenient (e.g., sanidines, in which the optic plane is parallel to the {010} cleavage). GRR2651 was oriented using a specially designed biaxial orientation device built on the principle of a spindle stage but at a macro scale with two axes of rotation (Thomas et al. 2014). For most of the samples, however, we estimated total integrated absorbance by measuring polarized spectra in three mutually perpendicular but not necessarily principal optical directions, following the approach taken by Johnson and Rossman (2004). A test of the accuracy of this method was made by Johnson and Rossman (2004) and is further discussed in the supplementary material. Hereafter we refer to the total (polarized) integrated absorbance measured this way or in principal orientations as Abs_{tot}, which can be converted to concentration using a modified form of the Beer-Lambert law:

$$c\ (\text{wt\% } H_2O) = Abs_{\mathrm{tot}} \times 1.805/[t \cdot D \cdot \mathrm{I}],$$

where t is the path length of the IR beam (in cm), D is the density of the mineral (in $g \cdot cm^{-3}$), I is the integral molar absorption coefficient in $L \cdot mol^{-1} \cdot cm^{-2}$ (also commonly symbolized as ε_i). When c is expressed as ppmw H_2O, I is replaced by I' (in $ppmw^{-1} \cdot cm^{-2}$). Johnson and Rossman (2003) derived values for I and I' of 107000 $L \cdot mol^{-1} \cdot cm^{-2}$ and 15.3 $ppmw^{-1} \cdot cm^{-2}$, respectively. In the discussion section we derive alternative values for these coefficients.

Infrared spectra were obtained in the main compartment of a Nicolet Magna 860 FTIR spectrometer, using a $LiIO_3$ Glan-Foucault prism polarizer (further analytical details are given in Mosenfelder et al. 2011 and are nearly identical to those in Johnson and Rossman 2003, 2004). In addition, we used the IR microscope to examine heterogeneity in microcline GRR968 using 50 μm apertures. Spline-fit baseline corrections with concave curvature, accounting for the tail of absorption from silicate overtone modes, were manually performed by the first author using

Nicolet's OMNIC software – both for our newly prepared samples and for spectra previously acquired by Johnson and Rossman (2003, 2004). Note that most spectra collected by Johnson and Rossman (2004) were fit with linear baselines; differences between those fits and new spline fits performed in this study are typically 3 to 5%. Uncertainties were assessed for each spectrum and propagated to determine the uncertainty on Abs_{tot}, as described in Mosenfelder and Rossman (2013a). This subjective evaluation of uncertainties takes into account factors such as signal: noise, the presence or absence of interference fringes, variations in silicate overtone band structure with crystallographic direction, and subtraction of bands interfering with fundamental O-H stretching vibrations. These include bands at ~4000 cm^{-1} due to the combination of low-energy lattice modes and OH or H_2O stretching (Johnson and Rossman 2003), as well as C-H absorption between ~2850 and 3050 cm^{-1}, attributed to residue left over from embedding the samples in poly(methyl methacrylate). Infrared spectra of this particular organic contaminant show that very little O-H is associated with the C-H bands (compared to other embedding media such as Crystalbond™ 509 or hard epoxies). Subtraction of the C-H bands amounts to much less than 1% of Abs_{tot} in most cases, while subtraction of the combination bands is dependent on crystal orientation and H speciation.

Electron probe microanalysis (EPMA)

EPMA data are given in the supplementary material. Some samples were analyzed previously using EPMA or SEM-EDS (Johnson and Rossman 2003, 2004). New analyses for other samples were obtained using a JEOL JXA8900R at the University of Minnesota. For these measurements we used an accelerating voltage of 15 keV, a beam current of 20 nA, and a spot size of 10 μm. Standards included synthetic $SrTiO_3$ (for Sr) and natural albite (for Na and Si), anorthite (for Ca and Si), microcline (for K), and hornblende (for Fe and Mg). Data processing followed the CITZAF method (Armstrong 1988). For the sake of comparing SIMS data among different samples, SiO_2 contents were recalculated by normalizing EPMA analyses to 100 wt% oxide totals.

SIMS

Our low blank SIMS methods for H and F analysis have been discussed in Mosenfelder et al. (2011) and Mosenfelder and Rossman (2013a, 2013b). Analytical details are identical to those in the latter two studies. Table 1 gives average blank corrected $^{16}OH/^{30}Si$ and $^{19}F/^{30}Si$ ratios for 5-14 analyses per sample; complete data for individual analyses are provided in the supplementary material. We converted $^{19}F/^{30}Si$ ratios (normalized for SiO_2) to F concentrations by calibrating against a suite of basaltic standard glasses (ML3B-G, KL2-G, BHVO-2G, and BCR-2G), using standard F concentrations from Guggino et al. (2011) (i.e. "model 2" in Mosenfelder and Rossman 2013a). The glasses were pressed in to the same indium mount as the feldspars, together with a suite of olivine standards (Mosenfelder et al. 2011) that were also measured in the same session. Our calibration line for the glasses (calculated using a York regression; York 1966) had a virtually identical slope (0.273) compared to Mosenfelder and Rossman (2013a). Although matrix effects for fluorine are unconstrained, we also measured the NIST high silica glasses SRM 610 and SRM 612 and note that they fall within the error envelope of the York regression for the basalts; if all six glasses are used instead of just the four basalts, the regression results in a lower slope (0.236) and correspondingly higher estimates for F, by about 14%. Full calibration data are given in the supplementary material.

For the sake of monitoring the H and F backgrounds in the vacuum and blank correcting SIMS measurements, we made "blank" standards at high temperature by diffusing these elements out from small cuboids made from two of the plagioclase crystals (GRR1389 and GRR145). The cuboids had dimensions of approximately 0.4 x 0.7 x 1.9 mm (GRR1389-HT) and 0.4 x 0.5 x 1.6 mm (GRR145-HT). The crystals were heated in three sets of successive experiments at 1050 °C, for 216, 96, and 90 hours, with FTIR spectra taken in between each step. The first two heating steps were performed in air in a muffle furnace and the last was done in a CO-CO_2 atmosphere in a Deltech™ gas-mixing furnace, at an oxygen fugacity corresponding to approximately one order of magnitude lower than the quartz-fayalite-magnetite buffer (cf. Mosenfelder and Rossman 2013a).

RESULTS

As delineated in the survey of Johnson and Rossman (2004), hydrogen can be contained in igneous feldspars in a variety of ways: as structurally bound OH with three distinct IR signatures (type I, IIa, and IIb), as structurally bound H_2O (types I, IIa, and IIb), in the form of NH_4^+ groups, and as H_2O in fluid inclusions or alteration phases. In this study we excluded feldspars (e.g., pegmatitic albites) with obvious spectroscopic evidence of fluid inclusions, type I OH, or NH_4^+. Representative IR spectra for the other modes of hydrogen incorporation are shown in Figure 1 and additional spectra for many of the samples we used are in Johnson and Rossman (2003, 2004); Figure 2 shows spectra for the one new sample (GRR2651) that we investigated. Furthermore, in the supplementary material we provide IR spectra for all samples together with our baseline corrections. Table 1 contains abbreviated SIMS, major element, and new FTIR data for all the samples, as well as the results of our refitting of original FTIR spectra from Johnson and Rossman (2003, 2004). Discrepancies among the FTIR results are discussed in detail in the supplementary material.

"Blank standards" and detection limits

Despite long annealing times for the two feldspars that we dehydrated for use as blank standards, neither crystal was fully dehydrated (as we expected from extrapolation of data from Johnson and Rossman 2013). Small peaks attributed to type IIa OH are present in GRR1389-HT and GRR145-HT at ~3200 cm^{-1} and ~3250 cm^{-1}, respectively. The peak location in GRR1389-HT is identical to that in the starting material (Fig. 1). GRR145-HT actually appears to have gained a small amount of H (on the order of 1 ppmw H_2O) compared to the starting material, suggesting some infinitesimal but significant fugacity of hydrogen under the high temperature dehydration conditions (even with the final step being in a CO-CO_2 atmosphere).

The integral absorbances for two directions in each crystal (the third direction was not measured) are given in Table 1, but these values represent transmission through the whole path length of each crystal and we assume that the H was concentrated toward the middle, following the typical pattern of diffusion profiles (Johnson and Rossman 2013). Indeed, SIMS data for GRR145-HT suggest that the surface was sufficiently dry for it to be effectively used as a blank standard, with $^{16}O^{1}H/^{30}Si$ ratios ranging from 0.00053 at the beginning of the session down to 0.00024 at the end. These ratios are slightly lower than those measured on our blank forsterite standard (GRR1017) during the same session ($^{16}O^{1}H/^{30}Si$ ranging from 0.00081 down to 0.00028). They are also identical to ratios measured at comparable time during the session in the starting material (GRR145), which was found to be dry below the FTIR detection limit. We elected to use GRR145-HT to monitor the background periodically and blank correct all the data, because F apparently diffused almost completely out of this crystal (whereas GRR145 has the second highest F content among all the feldspars we measured), making it suitable as well for blank correcting $^{19}F/^{30}Si$ ratios. $^{16}O^{1}H/^{30}Si$ ratios for GRR1389-HT were higher than both GRR145-HT and GRR2651 (see below), so it was not used for blank correction.

In previous studies we calculated detection limits for SIMS measurements using the classic analytical chemistry formulism of Long and Winefordner (1983) and regressions of SIMS data against H (expressed as H_2O) concentrations determined by FTIR, nuclear reaction analysis (NRA), or manometry. In this study we also tested the detection limit by deliberately measuring a sample with very low H content (GRR2651). IR measurements (Fig. 2) through thick sections (path lengths of 5.57 and 6.23 mm) of a well-oriented cuboid of this andesine yield Abs_{tot} corresponding to 1.4 ppmw H_2O using the calibration of Johnson and Rossman (2003); the concentration recalculated using a new value for I' determined in this study (see below) is half of that value. Six SIMS analyses gave an average blank-corrected $^{16}O^{1}H/^{30}Si = 0.00030 \pm 0.00003$ (2σ). Figure 3 shows raw data (after correction for dead time and background on the electron multiplier) for one of these analyses, bracketed immediately before and after by analyses on the blank standard GRR145-HT. This figure demonstrates that the average measured $^{16}O^{1}H/^{30}Si$ for GRR2651 is just above the limit of detection (LOD, 3σ above the blank), but below the limit of quantitation (LOQ, 10σ above the blank), as defined by Long and Winefordner. The consistency in measured ratios for this sample (10% RSD) suggests that quantification of H below the LOQ and much closer to the LOD is feasible with SIMS, when rigorous methods are used to achieve low H backgrounds (for this session we followed our previously documented procedures for cleaning the samples and mounting them in indium, baked the machine for 36 hours, and used an LN_2 cold trap).

Plagioclase and anorthoclase (type IIa OH)

The plagioclase and anorthoclase samples are all characterized by highly polarized IR spectra indicative of type IIa OH (Fig. 1a). Although the spectra show some variations, the strongest band in each sample is centered at ~3200 cm^{-1}. We used FTIR to look for H zoning but found none in these feldspars (spots were selected using 100-200 μm diameter, round apertures in the main compartment of the spectrometer). Our new FTIR results are consistent within mutual uncertainties with the originally published values of Johnson and Rossman (2003, 2004) in two cases: GRR145, which has no detectable H, and GRR580. For the other samples, we note discrepancies ranging from a few percent (for most samples) to as much as a factor of 10, and discuss the details in the supplementary material.

Five to ten SIMS analyses were acquired for each sample (Table 1). Reproducibility (2σ RSD) for $^{16}O^{1}H/^{30}Si$ ranged from 1% to 10% relative; the worst precision cited is for the low-H sample, GRR2651, with typical reproducibility for other samples between 2 and 6%. Fluorine varies from below the detection limit to 39 ppmw and is generally anti-correlated with H.

Figure 4 shows $^{16}O^{1}H/^{30}Si$ (normalized by multiplying by wt% SiO_2) plotted against Abs_{tot}, as determined for the actual crystals used for SIMS rather than the crystals originally studied by Johnson and Rossman (2003, 2004). The SIMS data are plotted against absorbance rather than H_2O concentration (as in previous studies) because we discuss revision of the IR absorption coefficient later in the paper. Moreover, these plots facilitate visualization of the differences among the different groups of feldspars. Parameters for ordinary least squares (OLS) and York (1966) regressions to the data are given in the supplementary material. The York fits take into account the different uncertainties in IR data (estimated subjectively) and SIMS data (based on reproducibility), which are assumed to be uncorrelated. Note that York regressions fit to the data in this way inherently lead to higher mean square weighted deviation (MSWD) and uncertainties on slope and intercept compared to regressions of SIMS data vs. H_2O concentration, because the uncertainty in the absorption coefficient is not propagated and thus the X-error bars are relatively small.

The data for anorthoclase (Fig. 4a) and plagioclase (Fig. 4b) can be fit separately with OLS regressions yielding correlation coefficients (r^2) of 0.997 and 0.954, respectively. The data also can be fit together, yielding a good correlation (r^2 = 0.969). One plagioclase sample (GRR1968 anorthite) constitutes an obvious outlier; if this sample is excluded from the regression the correlations improve significantly for plagioclase data alone (r^2 = 0.995) as well as all the data together (r^2 = 0.992), with slightly different but statistically insignificant slopes for the different fits; the MSWD of the corresponding York regressions also improves substantially (e.g., from MSWD = 95 to 15 for the combined data set; see supplementary material). Possible explanations for the deviation of GRR1968 from the trend include sample heterogeneity, misestimation of the sample absorbance, and a matrix effect due to its high Ca content; these possibilities are not exclusive. We discuss the first two possibilities in the supplementary material and the third in the discussion section.

Sanidine (type IIb OH)

Three sanidine crystals with type IIb OH were measured. GRR638 (Fig. 1b) and GRR2064 have similar spectra, with bands centered at ~3400 cm^{-1} and ~3250 cm^{-1} (with maximum absorption in *X*) and at ~3050 cm^{-1} (with maximum absorption in *Y*). The mean wavenumber of the sample (i.e. from the total absorbance) is ~3300 cm^{-1}. JV1 sanidine contains bands at similar positions, with additional, much less intense bands at ~3610 cm^{-1} and 3673 cm^{-1}. We collected five to seven SIMS analyses per sample and reproducibility for $^{16}O^{1}H/^{30}Si$ was 2% relative for the higher H-content samples and 16% for JV1, the lowest-H sample. Fluorine contents ranged from below detection limit to 4 ppmw, and are anti-correlated with H.

The SIMS and FTIR data (again, using revised values for Abs_{tot}; see supplementary material) for these feldspars are well correlated (r^2 = 1; Fig. 4c). Although the high r^2 value in this case is made somewhat less significant by the small number of data points compared to the fits for plagioclase and anorthoclase, the fit has a significantly higher calibration slope. The York regression improves substantially (from a MSWD of 4.2 to less than 1) if the lowest-H content sample (JV1) is excluded, but the slope and intercept are not significantly different; this may reflect a misestimation in Abs_{tot} for JV1 or some real but difficult-to-resolve difference in H content due to its slightly different H speciation compared to the other samples (if the absorption coefficient is frequency dependent).

Microcline and orthoclase (type I and II H_2O and/or type IIa OH)

We measured four K-feldspars with IR spectra dominated by bands attributed to structurally bound H_2O groups, covering a range from 30 to 1350 ppmw H_2O in previously estimated H concentrations. The two lowest-H content samples, GRR752 and GRR1618, also contain type IIa OH, while microclines GRR968 and GRR1281 contain only structurally bound H_2O.

Reproducibility for $^{16}O^{1}H/^{30}Si$ was 4-6% relative for all samples except for GRR752, for which reproducibility was 12% after the data were processed; unlike any other sample in this study, the analyses of this feldspar required extensive processing for contamination, apparently present not just on the sample surface but within the crystal (perhaps on cleavage planes). Following Mosenfelder et al. (2011), we used $^{12}C/^{30}Si$ ratios as a discriminant to eliminate "bad" cycles and recalculate $^{16}O^{1}H/^{30}Si$ ratios, and rejected five out of 14 analyses that yielded high overall ^{12}C counts.

SIMS and FTIR data for this group of samples are well correlated ($r^2 = 1$), and the slope of the calibration is significantly higher than both the plagioclase/anorthoclase data and sanidine/orthoclase data (Fig. 4d). The goodness of fit (but not the slope) of the York regression once again improves significantly if the lowest-H sample (GRR752) is excluded, probably for the same reasons as for the sanidine data. Figure 4d also shows the range (in the shaded box) of FTIR and SIMS data for a second sample chip of GRR968 that we knew was zoned in H before doing SIMS measurements; this sample is discussed in greater detail below but not included in the regressions.

Small discrepancies between our new estimates for Abs_{tot} in GRR752 and GRR1618 and those of Johnson and Rossman (2004) are outlined in the supplementary material. The discrepancies for the highest-H content microclines (GRR968 and GRR1281) are more complicated to rectify and our discussed here due to their potential significance for other workers measuring H_2O concentrations in microcline and importance for re-estimating the molar absorption coefficient originally determined by Johnson and Rossman (2003). Our re-estimates of Abs_{tot} for the originally measured spectra are consistent for GRR1281 but not for GRR968. In this latter case a transcription error appears to be responsible for the large discrepancy between the old value (13061 Abs_{tot}) and our new estimate (16429 Abs_{tot}). As shown in Figure 1d, our baseline corrections for these spectra include subtraction of absorption at high frequency that is attributed to a combination of low-energy lattice and H_2O stretching vibrations (Johnson and

Rossman 2003). This absorption is most prominent in *Y* spectra and uncertainties in its subtraction (modeled here as a single band, for simplicity) lead to the higher uncertainty (8-9%) in estimated absorbance in this direction, but *Y* is also fortuitously the direction with lowest absorbance.

An additional source of uncertainty in Abs_{tot} for GRR968 and GRR1281 comes from heterogeneities in H distribution, seen both in FTIR and SIMS. The heterogeneities are correlated to the presence of "turbid" versus "clear" regions in the crystals. The turbid regions are sample volumes with higher degrees of microperthitic exsolution. In Table 1 and Figure 1c we present previously unpublished FTIR data from Johnson and Rossman (2003) on a turbid section of GRR1281 that has 23% more absorbance, with the same IR band structure, compared to the "clear" section that was originally measured. The absorbance for the clear crystal is closer in absorbance to the new section we measured, and is presumably more representative of the clear crystal fragment that was crushed for use in NMR measurements. Note that the turbidity in these microclines is different than in other feldspars in which turbidity is caused by alteration (i.e., hydrous phases) and/or precipitation of fluid inclusions (Johnson and Rossman 2004; S□aby et al. 2012). In the samples studied here we see no spectroscopic evidence for fluid inclusions. Understanding of why incorporation of structurally-bound H_2O groups increases with increased exsolution in these samples requires further microstructural study.

We measured H by SIMS in two different sample sections of GRR968. One section ($^{16}O^{1}H/^{30}Si = 0.28 \pm 0.01$) was clear and showed no evidence for H zoning on the scale sampled by our FTIR measurements, while the other ($^{16}O^{1}H/^{30}Si = 0.30 \pm 0.02$) was variably turbid, showed considerable evidence for H zoning as seen in FTIR, and yielded twice as much variability in SIMS. Only two polarizations (close to *X* and *Z*) were measured in this second section, so for the sake of Figure 4d (and Table 1) Abs_{tot} is estimated by scaling, assuming that the *X* polarization accounts for 50% of the total absorbance (an average value for the other measured cuboids of GRR968). Abs_{tot} calculated this way ranges from 17146 to 22346 for this sample, with most of the apertured regions measured falling at the higher end of the range. The shaded area in Fig. 4d shows how this range of values plots against the other SIMS-FTIR data. They overlap with the other measurements shown, but are not used in the regression because it is not straightforward to correlate the zoning seen in FTIR with that in SIMS, due to the different sampling volumes (both in depth and lateral resolution) of these techniques.

DISCUSSION

IR absorption coefficient: a re-evaluation

Based on our results, we reassess the universal molar absorption coefficient determined by Johnson and Rossman (2003). In the following calculations we assume that the absorption coefficient is wavenumber dependent, based on the fact that our SIMS-FTIR calibration lines are significantly offset from each other for groups of feldspars with bands at different mean wavenumbers (Fig. 4d). An alternate interpretation is that the calibrations are offset due to SIMS matrix effects, a possibility we consider in a separate discussion section below. We proceed by first using our corrections to the original FTIR data of Johnson and Rossman to derive revised IR absorption coefficients (I and I') for samples containing type I and II H_2O based on the NMR measurements. Then, we calculate new I and I' values for the other feldspars with type IIa and IIb OH by using the microcline/orthoclase SIMS-FTIR calibration as a reference frame, assuming that there are no matrix effects.

Figure 5a shows a revised plot of the NMR results against Abs_{tot}. Here we use the original IR spectra of Johnson and Rossman (2003), but with our new baseline corrections; one exception is GRR638, for which we show our estimated absorbance from our new sample cuboid (with significantly higher absorbance in only one direction). The only other values that are significantly different are for GRR1280 plagioclase and GRR968 microcline (Table 1). The graph shows that our new estimate for GRR968 places that sample more in line with the origin and GRR1281 microcline, at higher H content. However, the data for plagioclase and sanidine still show a high degree of scatter, most likely due to uncertainties in the blank correction applied to these lower-H content samples. This precludes us from drawing meaningful conclusions from this plot alone as to whether the absorption coefficient can be applied universally to all feldspars.

We used a York regression (shown together with 95% confidence intervals in Fig. 5b) to calculate the molar absorption coefficient and associated uncertainty for the two microclines with type I and II H_2O (GRR968 and GRR1281). The regression is constrained to intercept within error of the origin by including a blank measurement of "zero" with a 50 ppmw uncertainty. This uncertainty was originally estimated for the measured blank of 100 ppmw based on assessment of the quantity of water that could be adsorbed on an anhydrous labradorite powder, which was measured by NMR and used to correct the NMR spectra. The uncertainty in the IR absorbance for GRR968 and GRR1281 is taken here to be 10% relative, which is a much higher uncertainty than our estimated uncertainties on Abs_{tot} (±2%) for the original spectra of these samples (Table 1). Our reasoning for this conservative estimate is that there may have been some heterogeneity in the crystalline material crushed up for NMR experiments, considering the range in Abs_{tot} that we have documented even among "clear" samples of GRR968 and GRR1281; for instance, the clear sample measured by Johnson and Rossman (2003) has 23259 Abs_{tot}, while a different clear

This is a preprint, the final version is subject to change, of the American Mineralogist (MSA)
Cite as Authors (Year) Title. American Mineralogist, in press.
(DOI will not work until issue is live.) DOI: http://dx.doi.org/10.2138/am-2015-5034

sample that we measured has 22096 Abs_{tot}, a difference of 5%; the corresponding difference for GRR1281 amounts to 8%. The resulting integral absorption coefficient I' from the slope of the York regression is 17.2 ± 1.6 $ppmw^{-1}{}_{H2O} \cdot cm^{-2}$ (2σ). This equates to I = 120,470 ± 11,360 $L \cdot mol^{-1}{}_{H2O} \cdot cm^{-2}$ if an average density for the microcline samples of 2.57 $g \cdot cm^{-3}$ is assumed (the measured densities were 2.556 and 2.585 $g \cdot cm^{-3}$, respectively, for GRR968 and GRR1281; Table 2 in Johnson and Rossman 2003). This new value for I' is higher than the original estimated value of 15.3 $ppmw^{-1} \cdot cm^{-2}$, although within mutual 2σ uncertainties. Note that using the lower estimated uncertainties for Abs_{tot} for GRR968 and GRR1281 results in a regression with essentially the same slope, yielding I' = 17.3 ±1.1 $ppmw^{-1}{}_{H2O} \cdot cm^{-2}$.

We now derive absorption coefficients for feldspars with type IIb OH (sanidine) and type IIa OH (plagioclase/anorthoclase) by equating their measured $^{16}O^{1}H/^{30}Si \times SiO_2$ values to H_2O concentrations (and then comparing those values to Abs_{tot}) using the microcline/orthoclase SIMS-FTIR calibration as a reference frame and the new calculated H_2O concentrations from the re-determined NMR calibration for microcline. For the sake of simplicity in these calculations (again performed using York regressions) we assume ten percent uncertainties on calculated H_2O concentrations and on the derived absorption coefficients, and we use densities of 2.56 $g \cdot cm^{-3}$ and 2.65 $g \cdot cm^{-3}$ for sanidine and plagioclase/anorthoclase, respectively. The resulting values for I' and I are:

I' = 21.3 ± 2.1 $ppmw^{-1}{}_{H2O} \cdot cm^{-2}$, I = 150,000 ± 15,000 $L \cdot mol^{-1}{}_{H2O} \cdot cm^{-2}$ (sanidine)

I' = 29.3 ± 3.0 $ppmw^{-1}{}_{H2O} \cdot cm^{-2}$, I =202,600 ± 20,260 $L \cdot mol^{-1}{}_{H2O} \cdot cm^{-2}$ (plagioclase/anorthoclase)

These values and the coefficient for microcline/orthoclase are plotted against typical mean wavenumber for the respective feldspars (calculated from spectra of GRR638, GRR1389, GRR968, and GRR1281) in Figure 6. This graph shows that I increases with decreasing frequency, in accord with other wavenumber-dependent calibrations determined both experimentally (Paterson 1982; Libowitzky and Rossman 1997) and theoretically (Balan et al. 2008). There is no reason to expect that the absorption coefficients for NAMs such as feldspars should be predicted exactly by any of the above cited functions, which were determined for stoichiometrically hydrous minerals, glasses, and/or various phases of water and water dissolved in organic solvents, glasses and quartz; large deviations from these calibrations and substantial variation have been found for many NAMs (e.g., Bell et al. 1995; Koch-Müller and Rhede 2010; Balan et al. 2012).

A more detailed treatment of the data would take into account the small variations in mean wavenumber among feldspars, rather than grouping them together into only three categories as we have done here, but such an analysis is unwarranted at the present time given the uncertainties involved. The NMR results on plagioclase are not reconcilable with the newly derived absorption coefficients. We have dismissed those results in this paper because of the scatter in the data and possible variability in the blank. However, the results on microcline are also subject to some uncertainty because of the possibility of heterogeneity in the samples, and our derivation of the new coefficients hinges on these data. Therefore there is clearly a need for additional determinations of H content in feldspars using low H-background, absolute methods such as NRA, proton-proton (p-p) scattering, or elastic recoil detection analysis (ERDA). Furthermore, an additional uncertainty that we have ignored so far in our discussion is the possibility that our SIMS-FTIR curves are offset because of matrix effects, a point we consider in the next section.

SIMS Matrix effects for hydrogen

Differences in ionization efficiency of hydrogen among different phases are most commonly attributed to variations in major element composition (e.g., Hervig and Williams 1988; Deloule et al. 1995; Ottolini et al. 1995, 2002; Hauri et al. 2002; King et al. 2002; Hervig et al. 2003; Koga et al. 2003; Aubaud et al. 2007; Mosenfelder and Rossman 2013a,b). As modeled by collision cascade models (e.g., Eiler et al. 1997; Hauri et al. 2006), these differences fundamentally influence the kinetic energy transfer between the implanted primary Cs^+ ions and the secondary ions that are formed prior to extraction into the optics of the mass spectrometer. The polyatomic ions ($^{16}O^1H^-$) that we analyze can form either through direct sputtering or via recombination above the surface of the sample, but in either case the secondary ion yield will be affected by the mass of the matrix atoms in the sample; the density and structure of the matrix may also affect this process but their effects are poorly constrained.

Our study has covered a wide range in compositional space for feldspars, but the differences in mean atomic mass of the different matrices are not, in fact, very large compared to many of the above cited studies due to the inherent trade offs in coupled substitutions of the tetrahedral cations (Al, Si) and A cations (Na, K, Ca). Nevertheless, prompted by the deviation of the SIMS data for the highest-Ca feldspar we measured (GRR1968) from the trend of the other plagioclases (Fig. 4b), we sought to quantify possible chemical matrix effects. Figure 7 shows the "SIMS calibration factor" for each measured feldspar as a function of the volatile-free mean atomic mass of the matrix. This calibration factor (cf. King et al. 2002) is simply the measured quantity ($^{16}O^{1}H/^{30}Si \times SiO_2/Abs_{tot}$) for each point in the graphs shown in Figure 4. The error in this factor is thus particularly high for the low H-concentration samples (GRR2651 andesine, JV1 sanidine, and GRR752 orthoclase), which may in any event deviate from the best-fit regressions to each data set because of differences in H speciation (or misestimation of Abs_{tot}), as discussed in the results section.

Taken altogether, the data plotted in Figure 7 suggest no systematic chemical matrix effect for feldspars. The data for microclines and anorthite, with similar mean atomic mass, vary by a factor of ~3 and the offset between the microcline/orthoclase data and the sanidine data cannot be explained by a mass-dependent matrix effect (supporting instead our model for frequency-dependent IR absorption coefficients). However, the figure also suggests that within the plagioclase and anorthoclase dataset alone (samples with type IIa OH only) there may be a non-linear matrix effect that could explain the offset of the GRR1968 data. The sense of the offset of GRR1968 from other plagioclases is consistent – despite large differences in methods – with the difference in H SIMS calibration lines measured by Deloule et al. (1995) for albitic/granitic versus anorthitic glasses, in which H_2O contents were measured by manometry (see their figure 5). It is also consistent with our previous suggestion of an intraphase matrix effect in clinopyroxenes, based on only one sample with relatively high mean atomic mass (Mosenfelder and Rossman 2013b). Further confirmation of this matrix effect obviously awaits study of other feldspars with high Ca content. Furthermore, there may be a mass-dependent matrix effect between the K-feldspars and the plagioclases that we cannot resolve with our present data set, introducing additional uncertainty to our derivation of frequency dependent IR absorption coefficients.

In addition to chemical effects, differences in structure of the matrix can influence the sputtering and ionization process. For instance, Eiler et al. (1997) documented differences in instrumental mass fractionation of oxygen isotopes between glasses and minerals of the same composition. However, these effects are very small (only up to ~3 per mil in the study of Eiler et al. 1997) and likely far below the resolution of H concentration measurements, as pointed out by Aubaud et al. (2007); for the small differences in structure among the feldspars, we also consider such effects unlikely to be relevant. A matrix effect related to the local bonding environment of the hydrogen atom itself is also conceivable, and potentially relevant in the present case because we have studied feldspars with both structurally bound H_2O groups and OH groups. Thus, microclines and sanidines with essentially the same major element composition but fundamentally different incorporation mechanisms for hydrogen might behave differently during the ionization process, explaining the difference in calibration slopes for these feldspars seen in Figure 4d and Figure 7. We cannot rule out this possibility but note that no such effect has been proposed, to our knowledge, to influence measurements of total H_2O in silicate glasses containing mixed OH and H_2O speciation. On the other hand, Hervig et al. (2003) present ambiguous results on a possible matrix effect between H-implanted glasses and glasses with structurally bound H_2O and/or OH; they saw an effect for basaltic glasses but not for rhyolites. Regardless, such a structural matrix effect could not readily explain the difference in calibration slopes for our samples with type IIa OH (anorthoclase and plagioclase) and type IIb OH (sanidine and orthoclase).

Finally, we can address the "interphase" matrix effect between feldspars and other NAMs because we measured, during the same session, a subset of olivine standards from Mosenfelder et al. (2011) mounted on the same sample block as our feldspars. Figure 8 shows a comparison of the olivine calibration assuming the Bell et al. (2003) IR calibration with the plagioclase calibration using the new value for I derived above (note that the nominal calibration slopes for other feldspars are statistically identical in this parameter space because they are all fixed to the reference frame of the microcline/orthoclase data). The slope of the calibration for olivine is within 5% of the calibration we showed in Mosenfelder and Rossman (2013a) from a previous session. While there is an apparently significant difference between the calibrations for olivine and feldspars, the lines are statistically indistinguishable if the new IR calibration of Withers et al. (2012) for olivine is employed instead to calculate their H concentrations. This is consistent with our discussion above about the effect of mean atomic mass on ionization efficiency, because the average molar mass of a typical mantle olivine (90 mol% forsterite) is 21, in the same range as the feldspars plotted in Figure 7.

Fluorine incorporation in feldspar

Studies of natural NAMs (Hervig and Bell 2005; Mosenfelder et al. 2011; Beyer et al. 2012; Mosenfelder and Rossman 2013a, 2013b) together with experimental work (Bernini et al. 2012; Beyer et al. 2012; Dalou et al. 2012; Crépisson et al. 2014) have demonstrated that these minerals can contain significant amounts of F, although the mechanisms of incorporation are still poorly understood. Although we know of no other modern, direct measurements of trace F in feldspars, previous studies provide hints that F may also be incorporated in this mineral group. Snow and Kidman (1991) measured the effect of F on solid-state alkali inter-diffusion in feldspar and inferred from the large enhancement of kinetics that F substitutes for O in the lattice of feldspar. Nakano et al. (2002) documented fluorite inclusions inside "butterfly" shaped microperthite exsolution domains in alkali feldspars. Their preferred interpretation ascribed these textures to precipitation of fluorite accompanying infiltration of F-rich hydrothermal fluids, but they also acknowledged the alternate possibility that the fluorite particles formed via exsolution of structurally-bound F.

The results of the present survey of igneous feldspars, from a variety of geological settings, suggest that amounts of F incorporated in feldspar are relatively low compared to other NAMs; concentrations for the samples studied here range from below detection limit to as high as 39 ppmw, but most samples contain less than 5 ppmw. Furthermore, the highest amounts of F that we measured (12 and 39 ppmw in GRR145 and GRR2651, respectively) were in the samples with the least amount of hydrogen. This rough anti-correlation between F and H is unlike other NAMs, particularly olivine, pyroxenes, and garnets. In those minerals, high F contents are generally only found in relatively H-rich crystals and F and H may form paired substitutions within the same defect sites (Mosenfelder and Rossman 2012; Crépisson et al. 2014).

Highly precise measurements of F are facilitated by its high ionization efficiency. Furthermore, F may diffuse more slowly through the lattice than H (based, for instance, on dehydration/defluorination of pyroxene "blank" standards in Mosenfelder and Rossman 2013a) and may therefore be better retained than H in volcanic feldspars. These two factors suggest that ultimately it may be feasible to use F contents of feldspars to constrain F contents of their parental magmas, once F distribution coefficients are known and calibration is improved; problems with the existing calibration method are discussed in Mosenfelder and Rossman (2013a).

Implications

In this study we have sought to improve the quantification of H in feldspars through a combination of analytical methods. SIMS and FTIR are both relative techniques relying on quantification of standards by absolute methods such as manometry, NMR, NRA, p-p scattering or ERDA. Nevertheless, as our calibration lines demonstrate, SIMS has the potential to yield important information about IR absorption coefficients when samples of similar composition but different hydrous speciation are compared. While there is still a need for further absolute measurements to determine H concentrations in feldspars, our study has implications for existing literature data and future work.

Our demonstration of high precision and low detection limits in SIMS analyses is encouraging for future studies of feldspar-melt H and F partitioning. For instance, Hui et al. (2013) used FTIR to measure ~2 and 6 ppmw H_2O in plagioclase crystals from lunar troctolites and anorthosites, respectively. Even such low amounts – if widespread in lunar rocks – can have significant implications for lunar magmatic history, and we have demonstrated the feasibility of measuring concentrations at this level using SIMS. Our results also point out some potential uncertainties particular to the measurement of H in An-rich, lunar-relevant feldspar compositions that bear further study.

One of the most important implications of the new absorption coefficients we derived for feldspars with varying H speciation is that H concentrations in plagioclase and anorthoclase may be systematically overestimated by a factor of about two in literature published since the work of Johnson and Rossman (2003). Thus, for instance, the feldspar-melt partitioning coefficients measured experimentally by Hamada et al. (2013) should be appropriately modified, and the solubilities determined for feldspars by Yang et al. (2012) may be similarly overestimated. While we are confident from this study that the absorption coefficient determined from NMR is not universally applicable to all feldspars, the lingering questions with regard to possible matrix effects in SIMS analysis need to be clarified with future work.

ACKNOWLEDGMENTS

Financial support for this research is gratefully acknowledged from: NSF grants EAR-0947956 and EAR-1322082 to G.R.R., EAR-1347908 to J.L.M., EAR-1161023 to Marc Hirschmann, the Gordon and Betty Moore Foundation, and the White Rose Foundation. We also thank Yunbin Guan for assistance with SIMS analyses; John Beckett for assistance with the gas-mixing 1-atm furnace; Anette von der Handt for assistance with EPMA at UMN; and Sheila Seaman and Associate Editor Adam Kent for helpful reviews of the manuscript.

REFERENCES

Armstrong, J.T. (1988) Quantitative analysis of silicate and oxide minerals, comparison of Monte Carlo, ZAF and $\phi(\rho z)$ procedures. In D.E. Newbury, Ed. Microbeam analysis, p. 239-246. San Francisco Press, San Francisco, CA.

Asimow, P.D., Stein, L.C., Mosenfelder, J.L., and Rossman, G.R. (2006) Quantitative polarized FTIR analysis of trace OH in populations of randomly oriented mineral grains. American Mineralogist, 91, 278-294.

Aubaud, C., Withers, A.C., Hirschmann, M., Guan, Y., Leshin, L.A., Mackwell, S., and Bell, D.R. (2007) Intercalibration of FTIR and SIMS for hydrogen measurements in glasses and nominally anhydrous minerals. American Mineralogist, 92, 811-828.

Balan, E., Refson, K., Blanchard, M., Delattre, S., Lazzeri, M., Ingrin, J., Mauri, F., Wright, K., and Winkler, B. (2008) Theoretical infrared absorption coefficient of OH groups in minerals. American Mineralogist, 93, 950-953.

Balan, E., Blanchard, M., Yi, H., and Ingrin, J. (2012) Theoretical study of OH-defects in pure enstatite. Physics and Chemistry of Minerals. DOI: 10.1007/s00269-012-0544-6.

Behrens, H. and Müller, G. (1995) An infrared spectroscopic study of hydrogen feldspar ($HAlSi_3O_8$). Mineralogical Magazine 59, 15-24.

Bell, D.R., Ihinger, P.D., and Rossman, G.R. (1995) Quantitative analysis of trace OH in garnet and pyroxenes. American Mineralogist, 80, 465-474.

Bell, D.R., Rossman, G.R., Maldener, J., Endisch, D., and Rauch, F. (2003) Hydroxide in olivine: a quantitative determination of the absolute amount and calibration of the IR spectrum. Journal of Geophysical Research, 108(2105), DOI:10.1029/2001JB000679.

Beran, A. (1986) A model of water allocation in alkali feldspar, derived from infrared-spectroscopic investigations. Physics and Chemistry of Minerals, 13, 306-310.

Beran, A. (1987) OH groups in nominally anhydrous framework structures: an infrared spectroscopic investigation of danburite and labradorite. Physics and Chemistry of Minerals, 14, 441-445.

Bernini, D., Wiedenbeck, M., Dolejs, D., and Keppler, H. (2012) Partitioning of halogens between mantle minerals and aqueous fluids: implications for the fluid flow regime in subduction zones. Contributions to Mineralogy and Petrology, doi:10.1007/s00410-012-0799-4.

Beyer, C., Klemme, S., Wiedenbeck, M., Stracke, A., and Vollmer, C. (2012) Fluorine in nominally fluorine-free mantle minerals: experimental partitioning of F between olivine, orthopyroxene, and silicate melts with implications for magmatic processes. Earth and Planetary Sciences, 337-338, 1-9.

Blundy, J., Cashman, K., and Humphreys, M. (2006) Magma heating by decompression-driven crystallization beneath andesite volcanoes. Nature, 443, 76-80.

Crépisson, C., Blanchard, M., Bureau, H., Sanloup, C., Withers, A.C., Khodja, H., Surblé, S. , Raepsaet, C., Béneut. K., Giura, P., and Balan, E. (2014) Clumped fluoride-hydroxyl defects in forsterite: implications for the upper-mantle. Earth and Planetary Science Letters, 390, 287-295.

Dalou, C., Koga, K.T., Shimizu, N., Boulon, J., and Devidal, J.L. (2012) Experimental determination of F and Cl partitioning between lherzolite and basaltic melt. Contributions to Mineralogy and Petrology, DOI 10.1007/s00410-011-0688-2.

Deloule, E., Paillat, O., Pichavant, M., Scaillet, B. (1995) Ion microprobe determination of water in silicate glasses: methods and applications. Chemical Geology, 125, 19-28.

Eiler, J.M., Graham, C., and Valley, J.W. (1997) SIMS analysis of oxygen isotopes: matrix effects in complex minerals and glasses. Chemical Geology, 138, 221-244.

Guggino, S.N. and Hervig, R.L. (2011) Synthesis and characterization of five new F-bearing basalt reference materials (Fba glasses): quantifying the fluorine content of the basaltic glass standards BCR-2G, BHVO-2G, GSA-1G, GSC-1G, GSD-1G, GSE-1G, ML3B-G, KL2-G, and ALV-519-4. American Geophysical Union, Fall Meeting 2011, abstract #V31C-2535.

Hamada, M., Kawamoto, T., Takahashi, E., and Fujii, T. (2011) Polybaric degassing of island arc low-K tholeiitic basalt magma recorded by OH concentrations in Ca-rich plagioclase. Earth and Planetary Science Letters 308, 259-266.

Hamada, M., Ushioda, M., Fujii, T., and Takahashi, E. (2013) Hydrogen concentration in plagioclase as a hygrometer of arc basaltic melts: Approaches from melt inclusion analyses and hydrous melting experiments. Earth and Planetary Science Letters 365, 253-262.

Hauri, E.H., Wang, J., Dixon, J.E.,, King, P.L., Mandeville, C., and Newman, S. (2002) SIMS analysis of volatiles in silicate glasses 1. Calibration, matrix effects and comparisons with FTIR. Chemical Geology, 183, 99-114.

Hauri, E.H., Shaw, A.M., Wang, J., Dixon, J.E., King, P.L., and Mandeville, C. (2006) Matrix effects in hydrogen isotope analysis of silicate glasses by SIMS. Chemical Geology, 235, 352-365.

Hervig, R.L. and Bell, D.R. (2005) Fluorine and hydrogen in mantle megacrysts. American Geophysical Union, Fall Meeting 2005, abstract #V41A-1426.

Hervig, R.L. and Williams, P. (1988) SIMS microanalysis of minerals and glasses for H and D. In: A. Benninghoven, A.M. Huber, ad H.M. Werner (Eds.), Proceedings of the 6th International Conference on Secondary Ion Mass Spectrometry (SIMS VI). Wiley, New York, N.Y., pp. 961-964.

Hervig, R.L., Mazdab, F.K., Moore, G., and McMillan, P.F. (2003) Analyzing hydrogen (H_2O) in silicate glass by secondary ion mass spectrometry and reflectance Fourier transform infrared spectroscopy. In: Devivo, B., Bodnar, R. (Eds.), Melt inclusions in volcanic systems: methods, applications, and problems. Developments in Volcanology. Elsevier, Amsterdam, pp. 83-103.

Hofmeister, A.M. and Rossman, G.R. (1985a) A model for the irradiative coloration of smoky feldspar and the inhibiting influence of water. Physics and Chemistry of Minerals, 12, 324-332.

Hofmeister, A.M. and Rossman, G.R. (1985b) A spectroscopic study of irradiation coloring of amazonite: structurally hydrous, Pb-bearing feldspar. American Mineralogist, 70, 794-804.

Hofmeister, A.M., and Rossman, G.R. (1986) A spectroscopic study of blue radiation coloring in plagioclase. American Mineralogist 71, 95-98.

Hui, H., Peslier, A.H., Zhang, Y., and Neal, C.R. (2013) Water in lunar anorthosites and evidence for a wet Moon. Nature Geoscience, 6, 177-180.

Johnson, E.A. (2005) Magmatic water contents recorded by hydroxyl concentrations in plagioclase phenocrysts from Mount St. Helens, 1980-1981. Geochimica et Cosmochimica Acta 69, A743.

Johnson, E.A. (2006) Water in nominally anhydrous crustal minerals: speciation, concentration, and geologic significance. In H. Keppler and J. R. Smyth, Eds., Water in Nominally Anhydrous Minerals, 62, p. 117-154. Reviews in Mineralogy and Geochemistry, Mineralogical Society of America, Chantilly, Virginia.

Johnson, E.A. and Rossman, G.R. (2003) The concentration and speciation of hydrogen in feldspars using FTIR and ^{1}H MAS NMR spectroscopy. American Mineralogist, 88, 901-911.

Johnson, E.A. and Rossman, G.R. (2004) A survey of hydrous species and concentrations in igneous feldspars. American Mineralogist, 89, 586-600.

Johnson, E.A. and Rossman, G.R. (2013) The diffusion behavior of hydrogen in plagioclase feldspar at 800-1000 °C: implications for re-equilibration of hydroxyl in volcanic phenocrysts. American Mineralogist, 98, 1779-1787.

King, P.L., Venneman, T.W., Holloway, J.R., Hervig, R.L., Lowenstern, J.B., and Forneris, J.F. (2002) Analytical techniques for volatiles: a case study using intermediate (andesitic) glasses. American Mineralogist, 87, 1077-1089.

Koch-Müller, M. and Rhede, D. (2010) IR absorption coefficients for water in nominally anhydrous high-pressure minerals. American Mineralogist, 95, 770-775.

Koga, K., Hauri, E., Hirschmann, M.M., and Bell, D. (2003) Hydrogen concentration analyses using SIMS and FTIR: comparison and calibration for nominally anhydrous minerals. Geochemistry, Geophysics, and Geosystems, 4, doi: 10.1029/2002GC000378.

Kronenberg, A.K., Yund, R.A., and Rossman, G.R. (1996) Stationary and mobile hydrogen defects in potassium feldspar. Geochimica Et Cosmochimica Acta 60, 4075-4094.

Libowitzky, E. and Rossman, G.R. (1996) Principles of quantitative absorption measurements in anisotropic crystals. Physics and Chemistry of Minerals, 23, 319-327.

Libowitzky, E. and Rossman, G.R. (1997) An IR absorption calibration for water in minerals. American Mineralogist, 82, 1111-1115.

Long, G.L. and Winefordner, J.D. (1983) Limit of detection. A closer look at the IUPAC definition. Analytical Chemistry, 55, 712A-724A.

Mosenfelder, J.L. and Rossman, G.R. (2012) Fluorine in the mantle: the role of nominally anhydrous minerals. American Geophysical Union, Fall Meeting 2012, abstract #DI54A-06.

Mosenfelder, J.L. and Rossman, G.R. (2013a) Analysis of hydrogen and fluorine in pyroxenes: I. Orthopyroxene. American Mineralogist, 98, 1026-1041.

Mosenfelder, J.L. and Rossman, G.R. (2013b) Analysis of hydrogen and fluorine in pyroxenes: part II. Clinopyroxene. American Mineralogist, 98, 1042-1054.

Mosenfelder, J.L., Le Voyer, M., Rossman, G.R., Guan, Y., Bell, D.R., Asimow, P.D., and Eiler, J.M. (2011) Analysis of hydrogen in olivine by SIMS: evaluation of standards and protocol. American Mineralogist, 96, 1725-1741.

Müller, G. (1988) Preparation of hydrogen and lithium feldspars by ion exchange. Nature 332, 435-436.

Nakano, S., Akai, J., and Sugaki, A. (2002) Fluorite particles inducing butterfly aggregates of incipient microperthite in alkali feldspar from a syenite, the Patagonian Andes, southern Chile. American Mineralogist, 87, 1377-1383.

Ottolini, L., Bottazzi, P., Zanetti, A., and Vannucci, R. (1995) Determination of hydrogen in silicates by secondary ion mass spectrometry. Analyst, 120, 1309-1313.

Ottolini, L., Cámara, F., Hawthorne, F.C., and Stirling, J. (2002) SIMS matrix effects in the analysis of light elements in silicate minerals: comparison with SREF and EMPA data. American Mineralogist, 87, 1477-1485.

Paterson, M.S. (1982) The determination of hydroxyl by infrared absorption in quartz, silicate glasses, and similar materials. Bulletin de Minéralogie, 105, 20-29.

Rossman, G.R. (2011) The Chinese red feldspar controversy: chronology of research through July 2009. Gems and Gemmology, 47, 16-30.

Seaman, S.J., Dyar, M.D., Marinkovic, N., and Dunbar, N. (2006) An FTIR study of hydrogen in anorthoclase and associated melt inclusions. American Mineralogist, 91, 12-20.

S□aby, E., Martin, H., Hamada, M., Śmigielski, M., Domonik, A., Götze, J., Joefs, J., Ha□as, S., Simon, K., Devidal, J.-L., Moyen, J.-F., and Jayananda, M. (2012) Evidence in Archaean alkali feldspar megacrysts for high-temperature interaction with mantle fluids. Journal of Petrology, 53, 67-98.

Snow, E. and Kidman, S. (1991) Effect of fluorine on solid-state alkali interdiffusion rates in feldspar. Nature, 349, 231-233.

Solomon, G.C., Rossman, G.R. (1979) The role of water in structural states of K-feldspar as studied by infrared spectroscopy. Abstracts with programs, Geological Society of America, 11, 521.

Solomon, G.C., Rossman, G.R. (1988) NH^{4+} in pegmatitic feldspars from the southern Black Hills, South Dakota. American Mineralogist 73, 818-821.

Thomas, T., Rossman, G.R., and Sandstrom, M. (2014) Device and method of optically orienting biaxial crystals for sample preparation. Review of Scientific Instruments 85, 093105.

Wilkins, R.W.T. and Sabine, W. (1973) Water content of some nominally anhydrous silicates. American Mineralogist, 58, 508-516.

Withers, A.C., Bureau, H., Raepsaet, C., and Hirschmann, M.M. (2012) Calibration of infrared spectroscopy by elastic recoil detection analysis of H in synthetic olivine. Chemical Geology, 334, 92-98.

Xia, Q.-K., Pan, Y., Chen, D., Kohn, S., Zhi, X., Guo, L., Cheng, H., and Wu, Y. (2000) Structural water in anorthoclase megacrysts from alkalic basalts: FTIR and NMR study. Acta Petrologica Sinica 16, 485-491.

(DOI will not work until issue is live.) DOI: http://dx.doi.org/10.2138/am-2015-5034

Yang, X.Z. (2012) An experimental study of H solubility in feldspars: Effect of composition, oxygen fugacity, temperature and pressure and implications for crustal processes. Geochimica Et Cosmochimica Acta 97, 46-57.

Yesinowski, J.P., Eckert, H., and Rossman, G.R. (1988) Characterization of hydrous species in minerals by high-speed 1H MAS-NMR. Journal of the American Chemical Society, 110, 1367-1375.

York, D. (1966) Least-squares fitting of a straight line. Canadian Journal of Physics. 44, 1079-1086.

Tables

Table 1. FTIR and SIMS data for feldspars

Appendices

Appendix 1. FTIR spectra

Appendix 2. EPMA data

Appendix 3. SIMS analyses of feldspar, June 2013

Appendix 4. SIMS analyses of F standards and olivine, June 2013

Appendix 5. Regression parameters for SIMS and NMR calibrations

Figure captions

Fig. 1. Representative mid-IR spectra for samples used in this study, showing different modes of hydrous speciation. All spectra are polarized with the E-vector parallel to the optical direction shown. Spectra are normalized to 1 cm sample thickness and offset for comparison. Spectra in **a-c** are shown without baseline correction. **a.** OH Type IIa typified by andesine GRR1389, showing consistent differences in all three polarizations between spectra originally collected by Johnson and Rossman (2003) and those taken on the sample used for SIMS in this study. **b.** OH Type IIb typified by sanidine GRR638. Spectra taken by Johnson and Rossman (2003) show good correspondence in *X* and *Z*, but not *Y*. **c.** Type I and II H_2O typified by microcline GRR1281 (original spectra from Johnson and Rossman 2003). Dashed curve is the *X* spectrum taken for a "turbid" portion of the sample. **d.** Close up of *Y* spectrum of GRR1281 shown in **c** showing baseline correction accounting for a band bear 3950 cm^{-1} assigned to a combination of low-energy lattice modes and H_2O stretching.

Fig. 2. Polarized mid-IR spectra of GRR2651. Uncorrected spectra, baselines, and corrected spectra shown by solid black, dashed, and grey lines respectively. Spectra are normalized to 1 cm sample thickness, labeled for polarization, and offset for comparison.

Fig. 3. SIMS analysis for GRR2651 bracketed by analyses of blank sample GRR145-HT, demonstrating the low background achieved during the session. The x-axis is arbitrarily labeled from 0 to 90 cycles through the mass sequence (30 cycles were acquired for each sample but the time corresponding to pre-sputtering and automated beam alignment is not represented on this graph). The solid black lines delineate the average value for each analysis, and the dashed lines represent the limits of detection and quantitation, based on the analyses of GRR145-HT.

Fig. 4. SIMS data plotted against Abs_{tot} for feldspars with different hydrous speciation. SIMS data are normalized by SiO_2 content, determined by EPMA. The point at the origin in each graph is the blank, measured on plagioclase. Error bars not shown are within the symbol size. **a.** Anorthoclase (type IIa OH). **b.** Plagioclase (open circles) and anorthoclase (filled squares), both with type IIa OH. Solid line is the OLS fit to all of the data; dashed line is the OLS fit to plagioclase data alone (in both cases with GRR1968 included in the regression). **c.** Sanidine (type IIb OH). Solid black line is the OLS fit to the data. Grey line is the OLS fit to the plagioclase data, illustrating the significant difference in calibration slope. **d.** Microcline and orthoclase with Type I/II H_2O and/or type IIa OH (see text for details). Grey shaded box represents the range of IR and SIMS data for the heterogeneous slab of GRR968 that was

measured. OLS regression shown by solid black line, with regressions for plagioclase and sanidine data also shown as grey lines.

Fig. 5. a. Revised NMR-FTIR calibration from Johnson and Rossman (2003), taking into account new absorbance estimates. Samples with significantly different new values are GRR968, GRR638, and GRR1281. Previous estimate for GRR968 shown by grey square with arrow pointing to new value; other previous values not shown for the sake of clarity. The line is an OLS regression to the new microcline data alone, constrained to pass through the origin. Error bars on NMR data discussed by Johnson and Rossman (2003); error bars on absorbance are given in Table 1, are lower than previously estimated, and within the symbol size for all points. **b.** York regression through microcline data and blank measurement, assuming larger error bars in absorbance (±10%) as discussed in text. 95% confidence intervals shown as dashed lines.

Fig. 6. Comparison of newly determined molar integral absorption coefficients for three groups of feldspars to the commonly used calibrations of Paterson (1982) and Libowitzky and Rossman (1997) and the theoretical prediction of Balan et al. (2008) for hydrous phases.

Fig. 7. SIMS "calibration factor" (see text) for each data point shown in Figure 4 as a function of mean atomic mass of the matrix, calculated from the EPMA data ignoring volatile content. Same symbols as in Figure 4 (diamonds, anorthoclase; open circles, plagioclase; squares, sanidine; closed circles, microcline and orthoclase). Dashed line is not a fit, but only a line meant as a guide to the eye for the trend of the plagioclase and anorthoclase data. The three points with the

relatively large error bars are andesine GRR2651, sanidine JV1, and orthoclase GRR752; all of these samples have the lowest measured H above the blank within their respective groups.

Fig. 8. Comparison of feldspar and olivine SIMS calibrations performed on the same mount during the same session. Data shown for four olivines originally studied by Mosenfelder et al. (2011). Grey line is a fit through the microcline/orthoclase data, but due to our assumptions about matrix effects the slopes of calibration lines for other feldspars are statistically identical. The dashed line represents the olivine calibration if the calibration of Withers et al. (2012) is used.

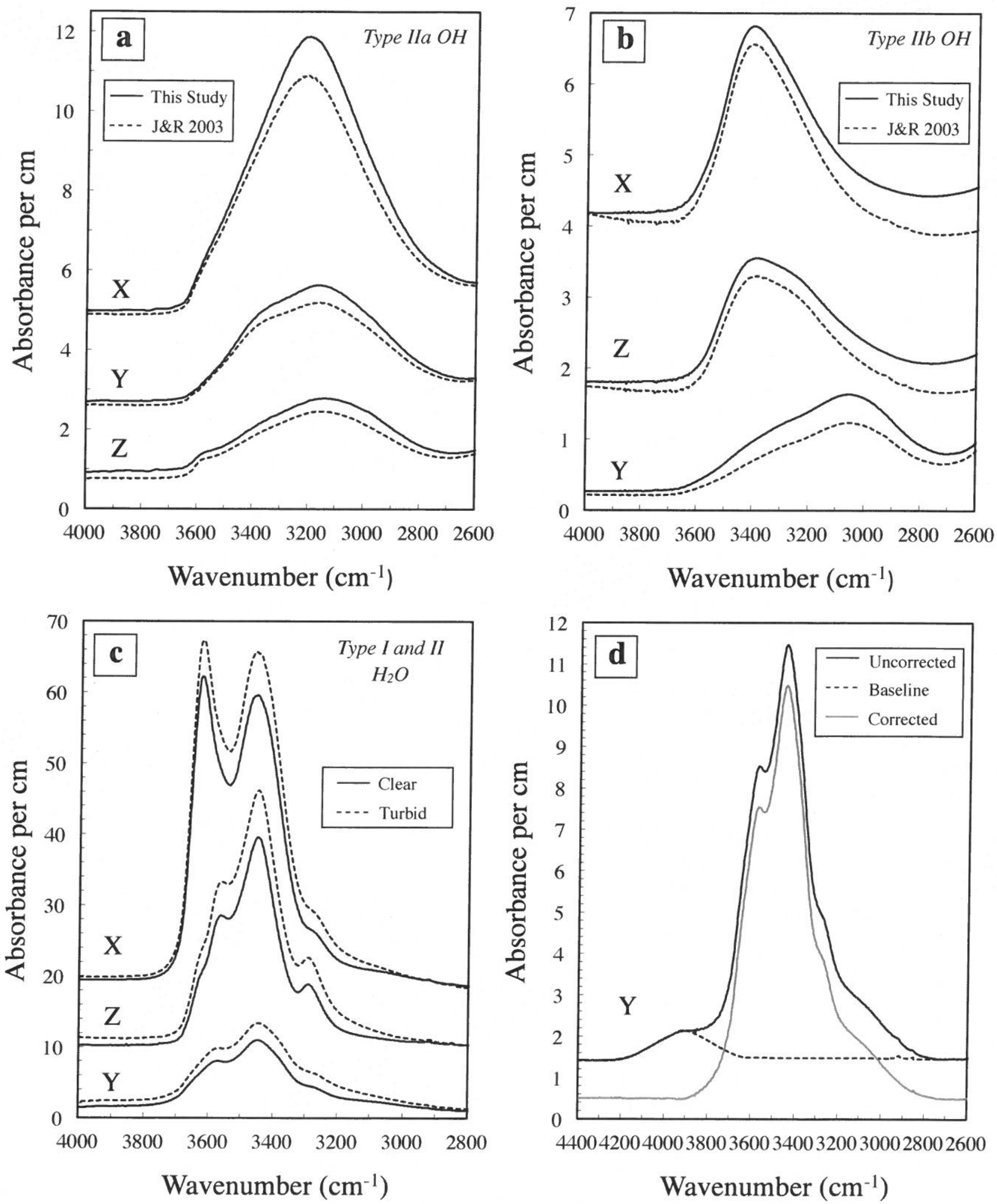

a
Type IIa OH
This Study
J&R 2003
X
Y
Z
Absorbance per cm
Wavenumber (cm-1)
b
Type IIb OH
This Study
J&R 2003
X
Z
Y
Absorbance per cm
Wavenumber (cm-1)
c
Type I and II
H2O
Clear
Turbid
X
Z
Y
Absorbance per cm
Wavenumber (cm-1)
d
Uncorrected
Baseline
Corrected
Y
Absorbance per cm
Wavenumber (cm-1)

Figure 1

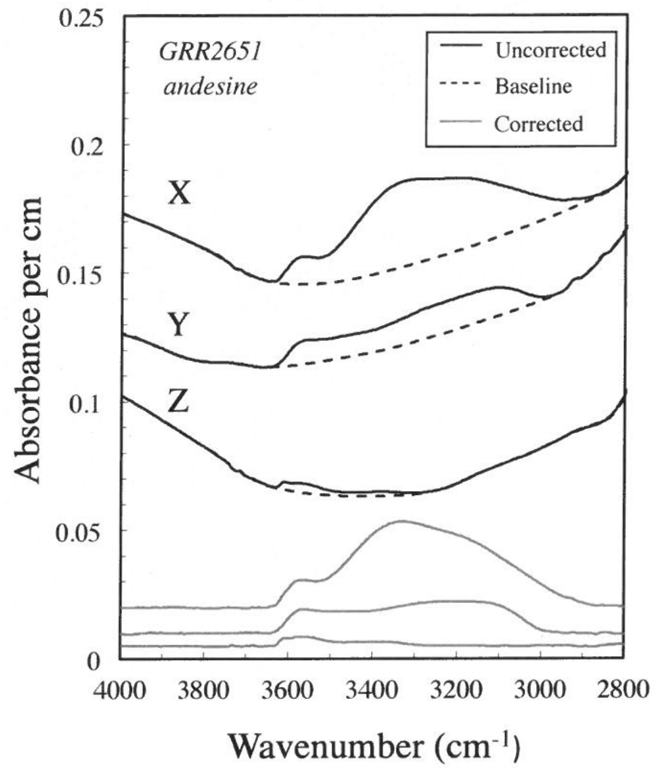
GRR2651
andesine
Uncorrected
Baseline
Corrected
X
Y
Z
0.25
0.2
0.15
0.1
0.05
0
Absorbance per cm
4000
3800
3600
3400
3200
3000
2800
Wavenumber (cm-1)

Figure 2

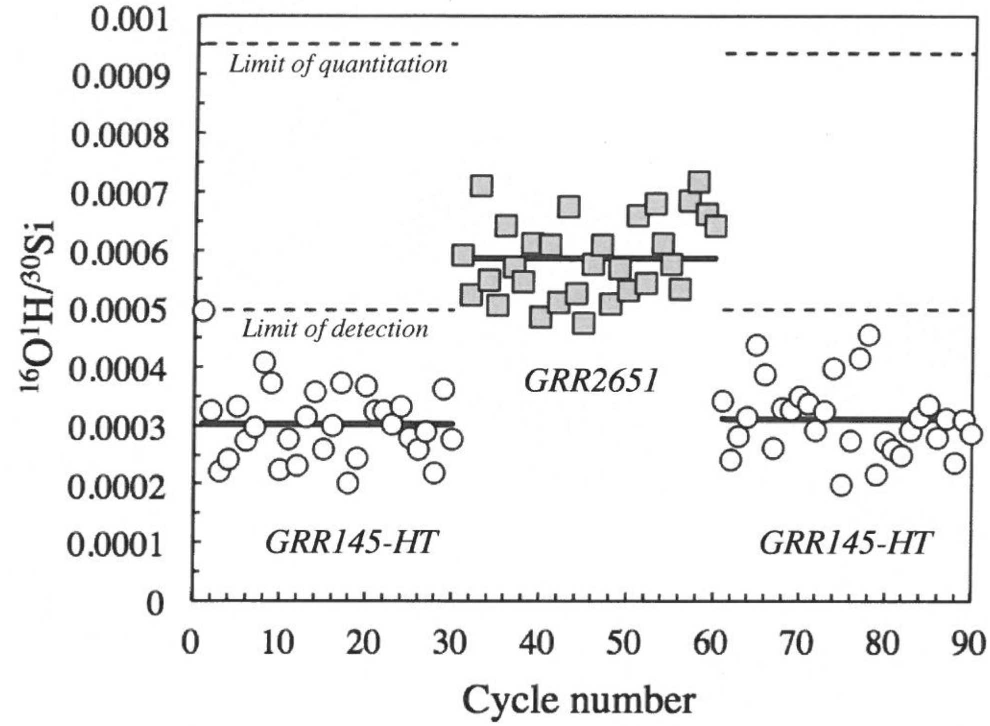

Limit of quantitation
Limit of detection
GRR2651
GRR145-HT
GRR145-HT
$^{16}O^{1}H/^{30}Si$
Cycle number
0.001
0.0009
0.0008
0.0007
0.0006
0.0005
0.0004
0.0003
0.0002
0.0001
0
0 10 20 30 40 50 60 70 80 90

Figure 3

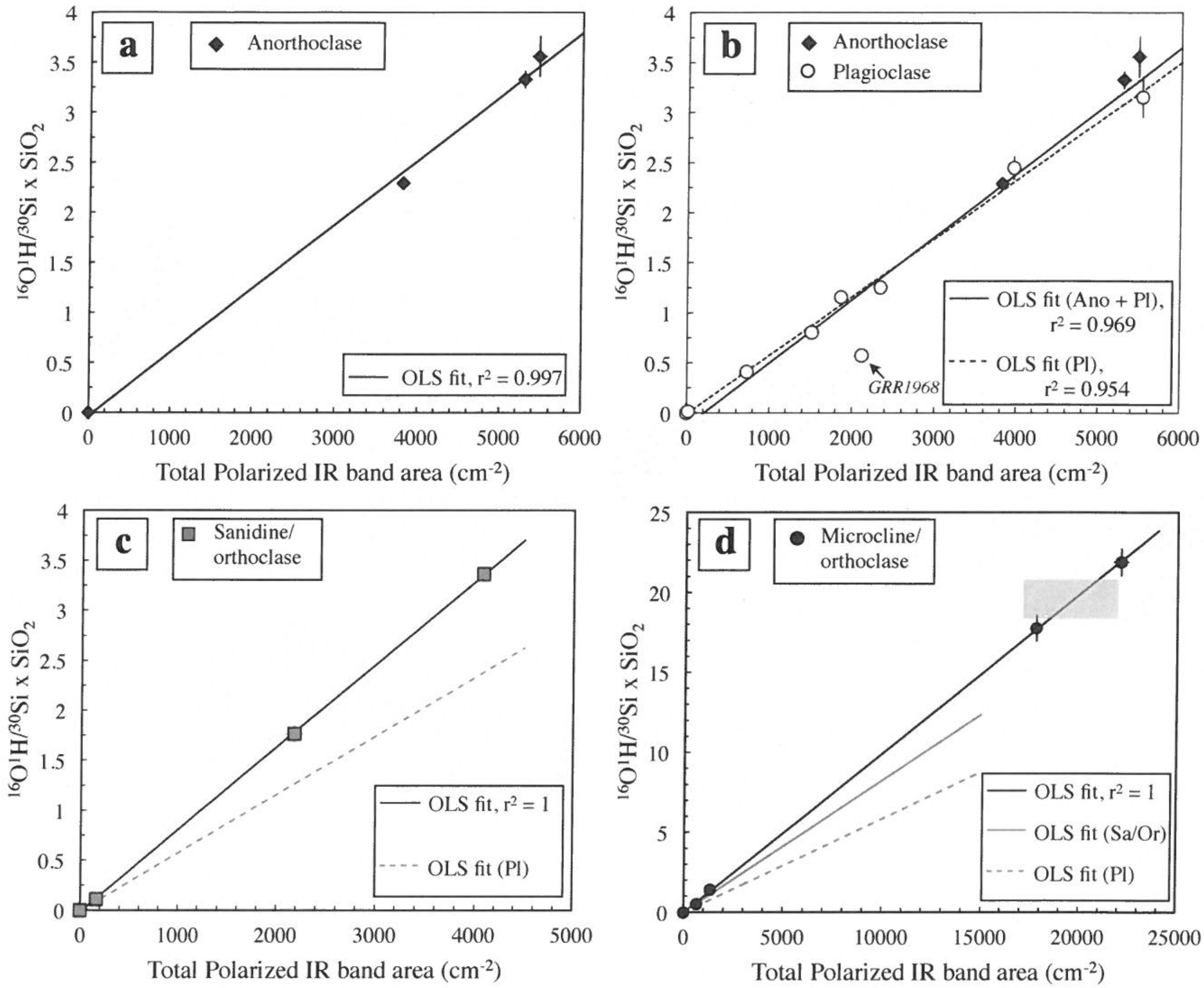
a
Anorthoclase
OLS fit, r² = 0.997
b
Anorthoclase
Plagioclase
GRR1968
OLS fit (Ano + Pl), r² = 0.969
OLS fit (Pl), r² = 0.954
c
Sanidine/ orthoclase
OLS fit, r² = 1
OLS fit (Pl)
d
Microcline/ orthoclase
OLS fit, r² = 1
OLS fit (Sa/Or)
OLS fit (Pl)
¹⁶O¹H/³⁰Si x SiO₂
Total Polarized IR band area (cm⁻²)

Figure 4

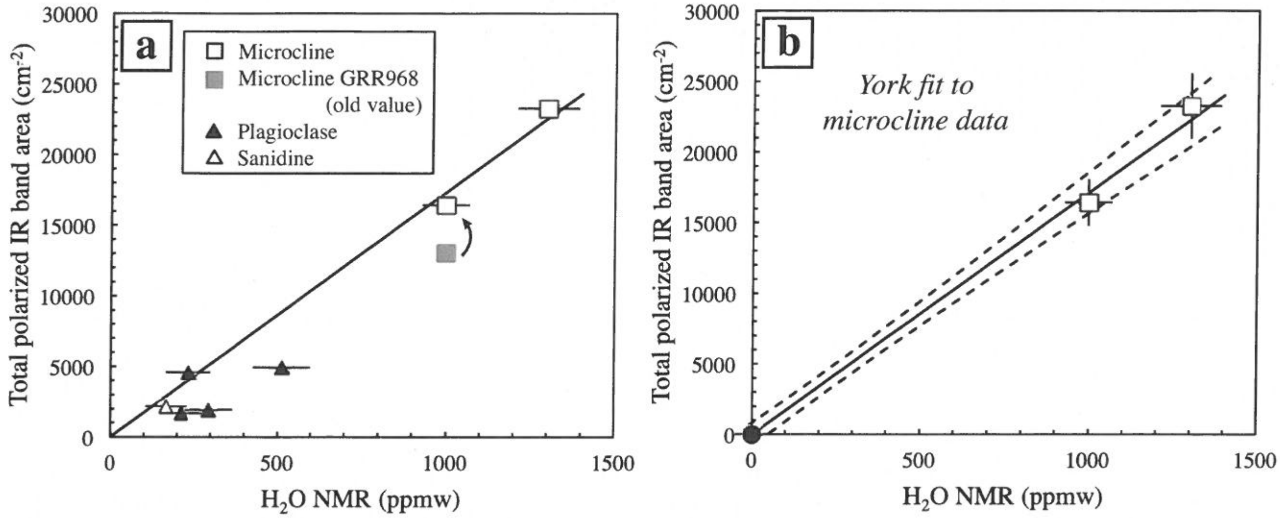

a
Microcline
Microcline GRR968
(old value)
Plagioclase
Sanidine
Total polarized IR band area (cm-2)
H2O NMR (ppmw)
0
5000
10000
15000
20000
25000
30000
0
500
1000
1500
b
York fit to
microcline data
Total polarized IR band area (cm-2)
H2O NMR (ppmw)

Figure 5

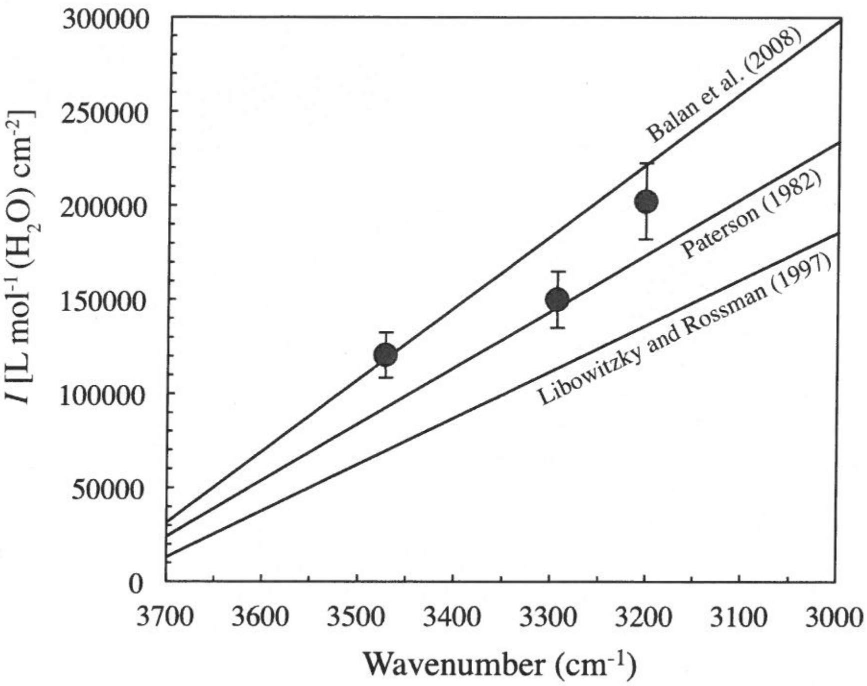
300000
250000
200000
150000
100000
50000
0
I [L mol^{-1} (H_2O) cm^{-2}]
Balan et al. (2008)
Paterson (1982)
Libowitzky and Rossman (1997)
3700
3600
3500
3400
3300
3200
3100
3000
Wavenumber (cm^{-1})

Figure 6

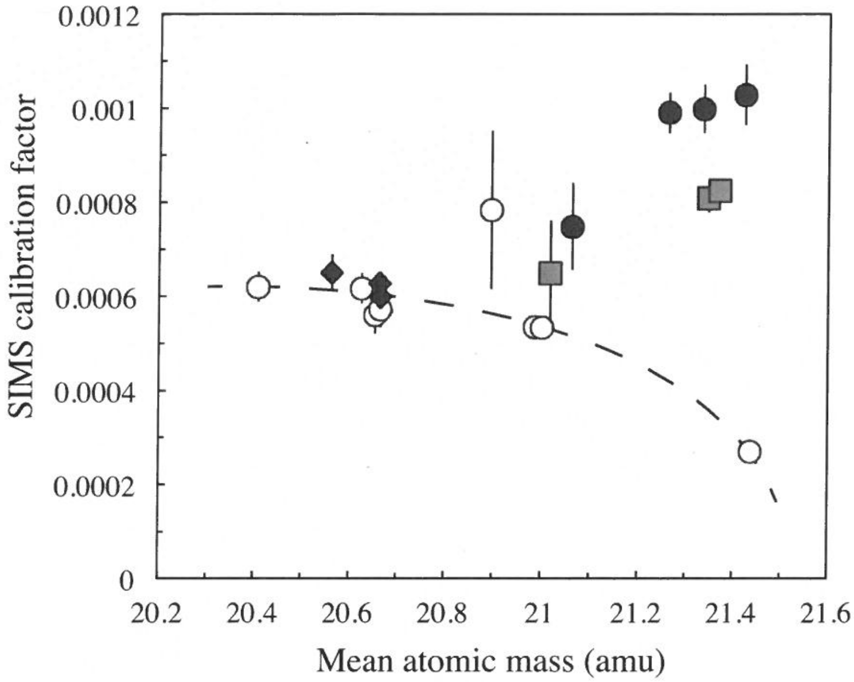

0.0012
0.001
0.0008
0.0006
0.0004
0.0002
0
SIMS calibration factor
20.2
20.4
20.6
20.8
21
21.2
21.4
21.6
Mean atomic mass (amu)

Figure 7

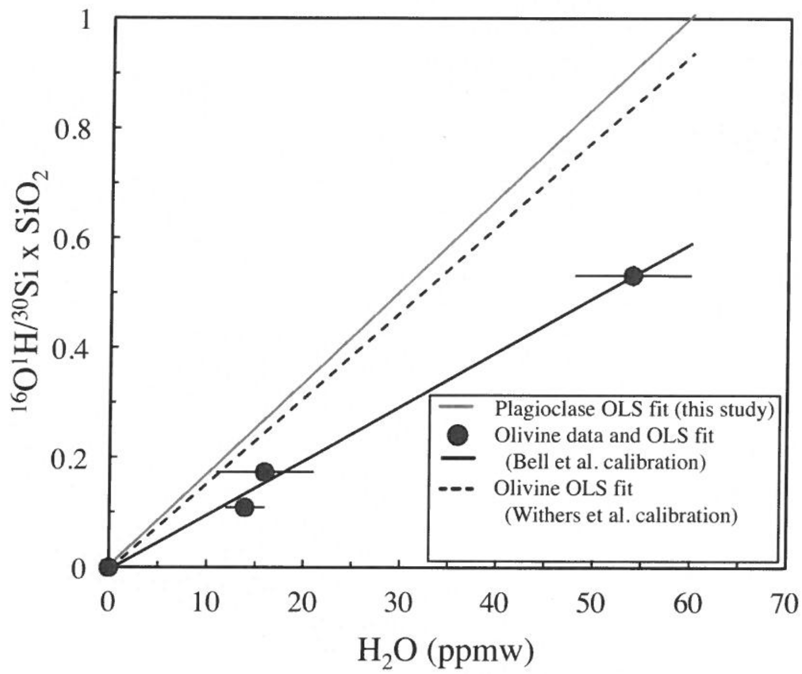

1
0.8
0.6
0.4
0.2
0
$^{16}O^{1}H/^{30}Si \times SiO_2$
0
10
20
30
40
50
60
70
H_2O (ppmw)
Plagioclase OLS fit (this study)
Olivine data and OLS fit
(Bell et al. calibration)
Olivine OLS fit
(Withers et al. calibration)

Figure 8

Table 1. Major element, SIMS, and FTIR data

Sample no.	Locality	Ab	An	Or	SiO_2	Abs/cm[a]			Abs_{tot}	Abs_{tot}	H_2O, JR03	H_2O, This study	No. of SIMS analyses	$^{16}O^{1}H/^{30}Si$	$^{19}F/^{30}Si$	Fluorine (ppm)[b]
					wt %	Pol 1	Pol 2	Pol 3	This Study	(J&R)[c]	(ppmw)[d]	(ppmw)[e]		(blank corrected)	(blank corrected)	
						Laboratory-dehydrated Plagioclase (OH IIa)										
GRR145-HT	Lake View, Lake Co., Oregon, U.S.A.	33.9	65.3	0.8	51.38	22(4)	20(1)	–	–	–	–	–	17	0.00053 – 0.00024[f]	0.00083 – 0.00048[f]	*n.d.*
GRR1389-HT	Halloran Springs, California, U.S.A.	63.5	32.4	4.1	59.20	57(17)	24(5)	–	–	–	–	–	5	0.0005(1)	–	*n.d.*
						Plagioclase (OH IIa)										
GRR145	Lake View, Lake Co., Oregon, U.S.A.	33.9	65.3	0.8	51.38	0	0	0	0	0	0	0	5	0.00052 – 0.00024[f]	0.063(2)	11.8(3)
GRR2651	China	47.1	50.2	2.7	54.86	14(4) **[X]**	6(2) **[Y]**	0.7(3) **[Z]**	21(4)	–	1.4(3)	0.7(2)	6	0.00030(3)	0.19(1)	39(2)
GRR1604	Cima volcanic field, California,	65.3	29.9	4.8	59.69	498(40)	160(16)	76(11)	734(44)		48(5)	25(3)	5	0.0069(2)	0.0072(5)	1.6(1)
						60(6)	*7.2(14)*	*6.0(20)*	*73(6)*	*60.2*	*4.8(6)*	*2.5(3)*				
GRR1968	Miyake Island, Japan	4.1	95.9	0.0	43.23	1004(30)	611(24)	511(31)	2126(49)		139(13)	73(8)	6	0.0133(8)	0.0005(1)	*n.d.*
						1158(23) ***[Y]***	*301(24)* ***[Z]***	*237(24)* ***[X]***	*1696(41)*	*1688*	*111(10)*	*58(6)*				
						642(19)	*580(35)*	*529(37)*	*1751(54)*[g]		*114(11)*	*60(6)*				
						808(57)	*757(53)*	*725(58)*	*2290(97)*[g]		*150(15)*	*78(9)*				
GRR1679	Spencer, Idaho, U.S.A.	40.6	57.0	2.4	52.52	654(218)	581(29)	276(19)	1511(45)		99(9)	52(5)	5	0.0154(3)	0.047(1)	9.1(2)
						822(16)	*233(19)*	*226(11)*	*1281(27)*	*1221*	*84(8)*	*44(5)*				
GRR580	South Carolina, U.S.A.	81.6	16.3	2.1	63.73	1106(22)	545(11)	216(17)	1867(30)		122(11)	64(7)	8	0.0182(9)	0.00072(4)	*n.d.*
						1215(24) ***[X]***	*514(15)* ***[Y]***	*206(21)* ***[Z]***	*1935(35)*	*1931*	*126(12)*	*66(7)*				
GRR25	Crater Elegante, Pinacate Ridge, Sonora, Mexico	37.4	61.0	1.6	51.70	1525(30)	436(22)	384(23)	2345(44)		153(14)	80(8)	5	0.0242(2)	0.0164(3)	3.11(6)
						1204(36)	*389(19)*	*416(17)*	*2009(44)*	*1905*	*131(12)*	*69(7)*				
GRR1280	Black Rock Pass, Nevada, U.S.A.	67.7	24.5	7.8	61.26	2567(64)	998(30)	398(32)	3963(78)		259(24)	135(14)	7	0.040(2)	0.0051(7)	1.1(2)
						2737(55) ***[X]***	*1554 (39)* ***[Y]***	*291(10)* ***[Z]***	*4582(68)*	*3979*	*299(28)*	*156(16)*				
GRR1389	Halloran Springs, California, U.S.A.	63.5	32.4	4.1	59.20	3228(65) **[X]**	1439(29) **[Y]**	851(25) **[Z]**	5518(75)		361(33)	188(19)	10	0.053(3)	0.0061(3)	1.33(7)
						2848(57) ***[X]***	*1306(39)* ***[Y]***	*777(31)* ***[Z]***	*4931(76)*	*4908*	*322(30)*	*168(17)*				
						Anorthoclase (OH IIa)										

GRR1554	Mt. Franklin, Daylesford, Victoria, Australia	70.8	5.1	24.0	64.59	2005(40)	1351(41)	472(38)	3828(74)		250(23)	131(14)	5	0.0355(8)	0.0115(8)	2.7(2)
						1919(38)	*1381(41)*	*537(43)*	*3837(71)*	*3649*	*251(23)*	*131(14)*				
GRR1276a	Aikins Quarry, Cima Volcanic Field, San Bernadino Co., California, U.S.A.	66.3	9.1	24.6	64.64	2702(54)	1877(38)	716(57)	5295(87)		346(32)	181(19)	5	0.051(1)	0.0032(4)	0.75(9)
						2486(51)	*1831(37)*	*745(60)*	*5062(87)*	*4921*	*330(31)*	*173(18)*				
GRR1277	Cone 32, McBride Province, Queensland, Australia	71.9	3.9	24.1	65.70	2813(56)	1968(39)	689(55)	5470(88)		358(33)	187(19)	8	0.054(3)	0.0029(3)	0.69(6)
						2015(40)	*1658(33)*	*652(52)*	*4325(73)*	*4129*	*283(26)*	*148(15)*				
							Sanidine (OH IIb)									
JV1	2nd cycle, Yellowstone Plateau Volcanic Field, U.S.A.	36.3	4.6	59.1	64.75	*79(6)* **[X]**	*49(7)* **[Z]**	*38(6)* **[Y]**	*166(11)*	*218*	*11(1)*	*8(1)*	7	0.0017(3)	0.017(2)	4.1(4)
GRR638	Eifel, Germany	14.0	4.5	81.5	63.58	904(18) **[X]**	703(35) **[Z]**	575(58) **[Y]**	2182(70)		143(14)	102(11)	5	0.0278(5)	0.0062(2)	1.44(5)
						919(28) **[X]**	*695(14)* **[Z]**	*410(41)* **[Y]**	*2024(52)*	*2075*	*132(13)*	*95(10)*				
GRR2064	Myanmar	5.7	0.6	93.7	64.67	1584(40)	1332(67)	1164(24)	4080(82)		267(25)	192(19)	5	0.052(1)	0.0006(1)	*n.d.*
						1305(33)	*1160(70)*	*1041(26)*	*3506(82)*	*3393*	*229(22)*	*165(17)*				
						Microcline/orthoclase (H_2O I/H_2O II/OH IIa)										
GRR752	Sri Lanka	32.5	2.2	65.3	64.58	263(18)	215(17)	181(13)	659(28)		43(4)	38(4)	14	0.009(7)	0.0002(1)	*n.d.*
													9[h]	0.0076(9)	0.00015(4)	*n.d.*
						215(17)	*153(12)*	*105(11)*	*473(24)*	*458*	*31(3)*	*28(3)*				
GRR1618	Kristallina, Switzerland (adularia)	8.4	4.7	86.9	63.26	612(12) **[X]**	466(23) **[Z]**	284(20) **[Y]**	1362(33)		89(8)	79(8)	9	0.022(1)	0.0005(1)	*n.d.*
						599(18) **[X]**	*466(23)* **[Z]**	*284(20)* **[Y]**	*1349(35)*	*1221*	*88(8)*	*78(8)*				
GRR968	Elizabeth R Mine, Pala, California, U.S.A.	9.7	0.0	90.3	64.26	9409(188)	5867(117)	2525(227)	17801(317)		1163(108)	1035(98)	10	0.28(1)	0.0012(1)	0.28(3)
						8553-11147[i]	6153-6546[i]		17146-22346[i]				10	0.30(2)	0.001(1)	0.3(2)
						8139(163) **[X]**	*5567(111)* **[Z]**	*2723(218)* **[Y]**	*16429(294)*	*13061*	*1074(100)*	*955(98)*				
GRR1281	White Queen Mine, Pala, California, U.S.A.	8.3	0.0	91.7	65.25	11586(232)	6993(140)	3517(281)	22096(390)		1444(135)	1285(122)	7	0.34(1)	0.0046(8)	1.1(2)
						12771(255) **[X]**	*7128(214)* **[Z]**	*3360(269)* **[Y]**	*23259(428)*[j]	*23232*	*1520(142)*	*1352(128)*				
						15152(303) **[X]**	*9244(185)* **[Z]**	*4282(343)* **[Y]**	*28678(494)*[k]		*1874(175)*	*1667(158)*				

Notes: n.d. = below detection limit; values in italics are for spectra originally obtained by Johnson and Rossman (2003,2004); uncertainties (in parentheses) are 2 SD

[a] Pol 1, Pol 2, Pol 3 are orthogonal polarizations; for crystals that were oriented, they represent *X*, *Y*, and *Z*, as labeled

[b] Fluorine determined using model 2 of Mosenfelder and Rossman (2013a)

[c] Value originally published by Johnson and Rossman (2003,2004)

[d] Value calculated using the original calibration of Johnson and Rossman (2003)
[e] Value calculated using new values for I determined in this study
[f] Ratios not corrected for blank, given as ranges from early to later in SIMS session
[g] randomly oriented cuboid prepared by Johnson and Rossman (2003)
[h] analyses processed for carbon contamination, see text
[i] only two directions measured in this section of sample studied by SIMS; numbers represent range in integrated absorbance, Abstot calculated as described in text
[j] clear crystal (used for NMR calibration)
[k] turbid crystal